Link between Acoustic and Hygrothermal Behavior of Hemp Shiv and Pith Composites

Mohamed Said Abbas, Antonin Fabbri, Mohammed Yacine Ferroukhi, Philippe Gle, Emmanuel Gourdon, Fionn Mcgregor

LINK BETWEEN ACOUSTIC AND HYGROTHERMAL BEHAVIOR OF HEMP SHIV AND PITH COMPOSITES

M. S. Abbas[1,2]*, A. Fabbri[1], M.Y. Ferroukhi[2], P. Glé[3], E. Gourdon[1], F. McGregor[1]

[1] LGCB-LTDS, UMR 5513 CNRS, ENTPE, Université de Lyon, F-69518, Vaulx-en-Velin, France
[2] LTDS, UMR 5513 CNRS, ENISE, Université de Lyon, St-Etienne, F-42023 France
[3] UMRAE, CEREMA, Université Gustave Eiffel, IFSTTAR, F-67035 Strasbourg, France

*Corresponding author; e-mail: mohamedsaid.abbas@entpe.fr

Abstract
Bio-based materials are an environmentally friendly alternative to classic construction materials, yet their generally low density can lead to poor acoustic properties. The acoustic performance of hemp shiv and sunflower pith composites is therefore analyzed using Kundt's tube. Although the loose aggregates present an exceptional sound absorbing behavior, it can be notably worsened in the presence of certain binders. The Transmission Loss is nevertheless enhanced by the binders, although it does not exceed 20 dB in most cases. For both properties, the type of binder has been found to be the most influential parameter.
Through the Kundt's tube method, it is also possible to determine the geometrical parameters of the composites' microstructure, which have been observed to be similar for materials presenting comparable hygrothermal properties and containing the same binder. In a previous work, an experimental correlation was found between the thermal conductivity and the interparticle porosity of the aforementioned composites, which is compared to theoretical thermal conductivity models from literature without finding any apparent correspondence.

Keywords:
Acoustic properties; Hemp shiv; Hygrothermal properties; Kundt's tube; Pith composites

1 INTRODUCTION

The increasing awareness about the environmental footprint of human activity has motivated the search for innovative construction materials, since the emissions linked to the construction and the operation of buildings represent 38% of the global $CO_{2equivalent}$ emissions (International Energy Agency & UN Environment Programme, 2020). Bio-based materials, which are defined as non-alimentary products, totally or partially derived from biodiversity, represent a very promising alternative to traditional materials for two reasons: on the one hand, they have a lower embodied energy (Cornaro et al., 2020; D'Alessandro et al., 2017; Lupíšek et al., 2015) due to their natural origin and, on the other, they present a good hygrothermal (Cérézo, 2005; Chamoin, 2013) behavior including a low thermal conductivity, which helps to reduce thermal losses and, therefore, energy consumption (Ahmad et al., 2020; Mnasri et al., 2020).

In a context in which the noise of transport, of building equipment and of the city are part of everyday life, the acoustic insulation of houses and buildings is another essential feature of construction materials. Regulations such as the NRA 2000 for multi-family housing in France establish the legal requirements for sound insulation. Since bio-based building materials have by nature a lower mass effect, a thorough study of their acoustic behavior is necessary.

The acoustic performance of materials has two main functions. On the one hand, the limitation of sound reflections, thus the reduction of reverberations. This function is linked to the phenomenon of absorption. On the other hand, the ability to reduce the transmission of sound. This is related to the phenomenon of acoustic attenuation and can be accomplished by three mechanisms of dissipation: viscous dissipation, thermal dissipation, and structural dissipation. When the material is too heavy or too rigid, the acoustic waves are not able to transmit their vibrations to it and the structural dissipation becomes negligible.

In this paper, the acoustic behavior of hemp shiv and sunflower pith composites, bio-based materials that have already been studied in previous works (Abbas et al., 2020, 2021, 2019), is analyzed. This is done using a Kundt's tube, a method that is all the more interesting since it allows the determination of the geometrical parameters of the microstructure of the porous medium thanks to acoustic models such as Johnson-Champoux-Allard (JCA) (Cambonie & Gourdon, 2018; Glé, 2013; Gourdon et al., 2015).

2 MATERIALS AND METHODS

2.1 Materials

Aggregates

Five types of vegetal aggregates have been used in this study: a sunflower pith called 'S' with origin France and four types of hemp shiv. 'F' and 'H' originate from France, 'UK' comes from United Kingdom and 'G' comes from Germany. The dimensions and the average skeletal density of each type of aggregate are shown in Tab. 1.

Tab. 1: Main characteristics of the aggregates

Aggregate	H	S	F	UK	G
$\rho_{skeletal}$ [kg/m^3]	769.2±2	1400±1	964±2	1104±7	1213±10
Length [mm]	4.1±NA	-	1.30±0.78	1.71±1.00	1.53±1.02
Width [mm]	7.6±NA	-	4.61±3.09	6.17±4.07	5.82±4.79
Diameter [mm]	-	3.73±2.02	-	-	-

Binders

Four binders were used in this experimental campaign: C2, which stands for a hydraulic lime mixed with calcareous charges and some admixtures; a 95% pure aerial lime called H98; CLIN, which consists of Portland cement with a low content of Al_2O_3 and which does not contain tricalcium aluminate; and C1, whose commercial denomination is PF70, and which is made of 75% aerial lime, 15% hydraulic lime and 10% pozzolanic lime.

Bio-based composites

From these components, 9 different composites were manufactured at 23°C and 50%RH. Their formulation and dry density are detailed in Tab.2. All samples had the same dimensions (10 cm diameter and 5 cm thick) and were manufactured in cylindrical formworks. C2-S and C2-H+S samples where sprayed, whilst all the rest were cast. In order to obtain very precise dimensions and a good surface condition, both necessary for the acoustical tests, formworks need to be slightly bigger than the desired dimensions (about 10,5 cm of diameter and 5,15 cm high), then the samples must be carefully filed with sandpaper.

Tab. 2: Summary of the composites' formulation and dry density

Formulation	C2-H*	C2-S	C2-H+S	H98-G	H98-UK	H98-F	CLIN-UK	CLIN-G	C1-F
Aggregate/binder mass ratio (-)	0.33	0.10	0.17 (H) 0.06 (S)	0.5	0.5	0.5	0.5	0.5	0.5
Water/binder mass ratio (-)	0.88	0.80	1.07	1.86	1.64	1.70	1.03	1.09	1.44
Dry density ρ_{dry}(kg/m^3)	600	550	590	353	392	380	401	374	433

The samples H98-G, H98-UK, H98-F, CLIN-UK, CLIN-G and C1-F belong to the experimental campaign of (Glé, 2013).

2.2 Methods

Hygrothermal properties

The thermal conductivity (λ) of the samples has been determined using the hot wire probe of the FP2C device and following the ISO 8894-2 standard (International Organization for Standardization, 2007). The test has been conducted 100 days after manufacture and at ambient conditions of 23°C (±1°C) and 50%RH (±2%RH).

The water vapor permeability (δ_p) has been measured through the wet cup method according to the standard NF EN ISO 12572 (International Organization for Standardization, 2016) and following (McGregor et al., 2014)'s method for the preparation of the samples. The relative humidity inside the cups was established at 85%RH using a saturated aqueous solution, and the samples were introduced in a climatic chamber regulated at 50%RH and 23°C.

The moisture buffering value (MBV) was determined following the NordTest protocol (Rode et al., 2005), during which the temperature was established at 23°C. The ideal moisture storage capacity is deduced from these results using:

$$\zeta_{\text{ideal}} \approx 0.65\,\mu\left(MBV_{practical}\right)^2 \quad (1)$$

Where $\mu = \frac{\delta_a}{\delta_p}$ [-] stands for the moisture resistivity factor and δ_a [kg/(m.s.Pa)] stands for the water vapor permeability of air.

Acoustic properties

The Kundt's tube or impedance tube technique was used to determine the acoustic properties of the samples using the 3-microphone no-cavity configuration as described in (Iwase et al., 1998). The layout of the test bench is presented in Fig. 1, which shows a steel cylinder with a loudspeaker blocking one end and with a plastic rigid backing blocking the other end. The sample is placed inside the tube, next to the rigid backing, and the three microphones allow the determination of the different properties.

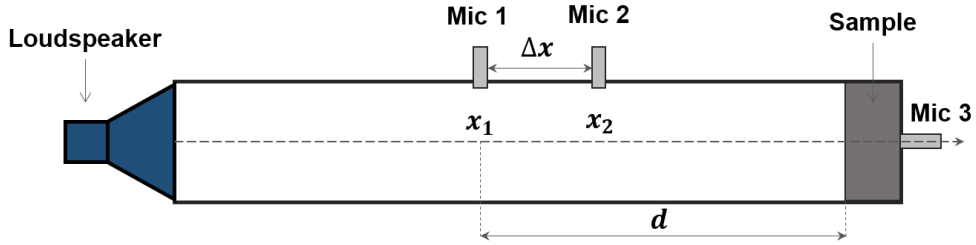

Fig. 1: Kundt's tube with the three microphones and no-cavity configuration

More specifically, the tube used in this work is a B&K Type 4106 with a 100 mm diameter and 1000 mm long. In the figure, the distance between microphones Δx is 5 cm and the distance between the first microphone and the nearest side of the sample, noted d, is 37 cm. The loudspeaker is powered through a B&K type 2706 amplifier, while a B&K type 2690 conditioning amplifier treats the signal coming from the microphones. A National Instruments NI PXI-1031 board generates the sound signals.

This method yields the values of the sound absorption coefficient α [-], which represents the part of the acoustical energy of an incidental wave that is not reflected by the material; the transmission loss or TL coefficient [dB], which quantifies the energy lost by the acoustical wave when travelling through the material; as well as the intrinsic acoustic parameters: ρ the dynamic density and K the dynamic incompressibility modulus, which are determined following the method described by (Utsuno et al., 1989).

The sound absorption coefficient α is determined through the following formulas:

$$H_{12} = \frac{p_2}{p_1} \tag{2}$$

$$\mathcal{R} = \frac{H_{12} - e^{-jk_0\Delta x}}{e^{jk_0\Delta x} - H_{12}} e^{2jk_0 d} \tag{3}$$

$$\alpha = 1 - |\mathcal{R}|^2 \tag{4}$$

Where Δx and d are measured in meters, $k_0 = {}^{\omega}/_{c_0}$ is the wave number in air, ω [rad] is the angular frequency and c_0 [1/m] the speed of sound.

Regarding the Transmission Loss coefficient TL, it is determined as follows:

$$TL = -10\log(|Tr|^2) \tag{5}$$

$$Tr = \frac{2e^{jk_0 d}}{2\cos(kd) + j\sin(kd)\left(\frac{Z_c}{Z_0} + \frac{Z_0}{Z_c}\right)} \tag{6}$$

In which Tr stands for the transmission coefficient, Z_0 the characteristic impedance of free air, k the wave number of the medium and Z_c the characteristic impedance of the medium.

Geometrical parameters

From ρ and K, it is possible to deduce the geometrical parameters of the porous media through the inversion of the Johnson-Champoux-Allard or JCA model (Champoux & Allard, 1991; Johnson et al., 1987) and of the Zwikker and Kosten model (Zwikker & Kosten, 1949). The first parameter is the air resistivity σ [N.s/m^4], which describes a material's ability to slow a fluid flowing through it per unit thickness, is estimated through the formula presented in (Panneton & Olny, 2006) and which derives from the JCA model:

$$\sigma = \lim_{\omega \to 0} -\omega \Im(\rho) \tag{7}$$

The second parameter is the interparticle porosity ϕ_{inter} [-], defined as the air gaps left between several aggregate particles and between the aggregate particles and the binder and determined through formulas (8) and (9), which are based on the Zwikker and Kosten model:

$$\phi_{inter} = \lim_{\omega \to 0} \frac{P_0}{\Re(K)} \tag{8}$$

$$\phi_{inter} = \lim_{\omega \to \infty} \frac{\gamma P_0}{\Re(K)} \tag{9}$$

The tortuosity α_∞ [-] represents the sinuosity of the porous structure or the ratio between the trajectory of the acoustic wave and the theoretical straight-lined trajectory, and it is estimated through (Panneton & Olny, 2006)'s formula, which derives from the JCA model:

$$\alpha_\infty = \frac{\phi}{\rho_0}\left[\Re(\rho) - \sqrt{\Im(\rho)^2 - \frac{\sigma^2}{\omega^2}}\right] \quad (10)$$

The viscous characteristic length Λ [m] is an estimation of the radius of the interconnexions between pores, where the viscous effects mainly take place, and is calculated through (Panneton & Olny, 2006)'s formula, based on the JCA model:

$$\Lambda = \frac{\alpha_\infty}{\phi}\sqrt{\frac{2\rho_0\mu}{\omega\Im(\rho)\left(\rho_0\frac{\alpha_\infty}{\phi} - \Re(\rho)\right)}} \quad (11)$$

Lastly, the thermal characteristic length Λ' [m] estimates the radius of the greater section of the pores, which is associated to the dissipation of energy of the acoustic waves through the heat exchange between the fluid and the solid matrix. It can be calculated using (Olny & Panneton, 2008), which is also based on the JCA model:

$$\Lambda' = \delta_t\sqrt{2\left[-\Im\left(\left(\frac{1-\phi K/(\gamma P_0)}{1-\phi K/P_0}\right)^2\right)\right]^{-1}} \quad (12)$$

The total open porosity ϕ_{total} is measured using a nitrogen pycnometer, while the intraparticle porosity ϕ_{intra}, defined as the pores inside the binder paste and inside the aggregate, is deduced from the following formula:

$$\phi_{total} = \phi_{inter} + (1 - \phi_{inter})\phi_{intra} \quad (13)$$

3 RESULTS AND DISCUSSION

3.1 Results

Acoustic properties

The results of the sound absorption coefficient (α) and of the Transmission Loss (TL) coefficient of two aggregates, S and H, and of the nine composites are shown in Fig. 2-4.

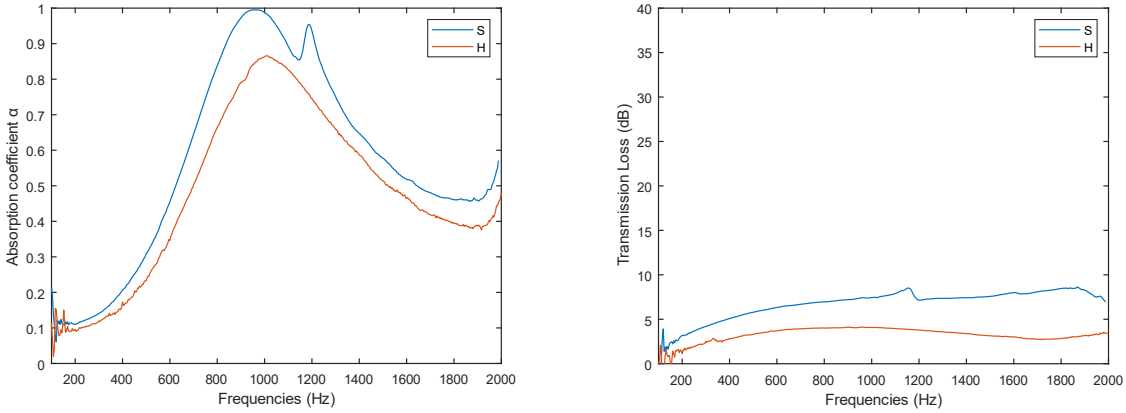

Fig. 2: Sound absorption coefficient (left) and Transmission Loss coefficient (right) of the aggregates S and H.

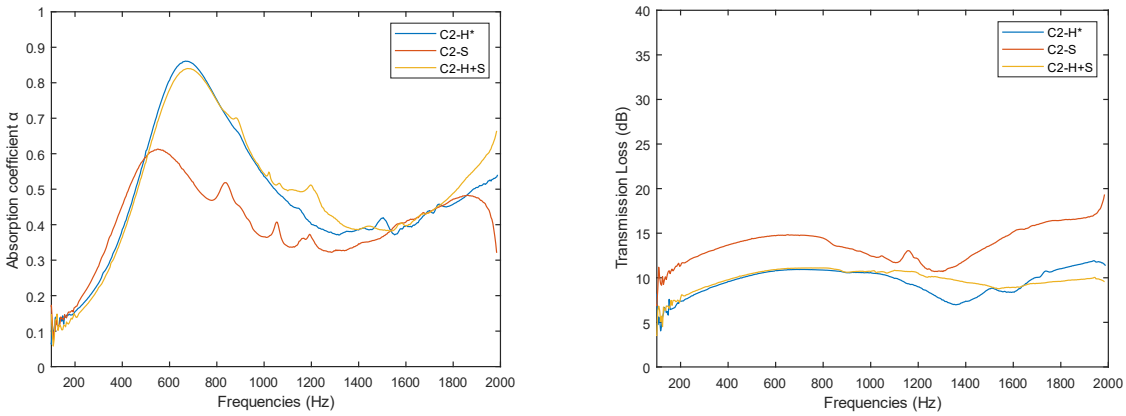

Fig. 3: Sound absorption coefficient (left) and Transmission Loss coefficient (right) of the composites C2-H, C2-S and C2-H+S.*

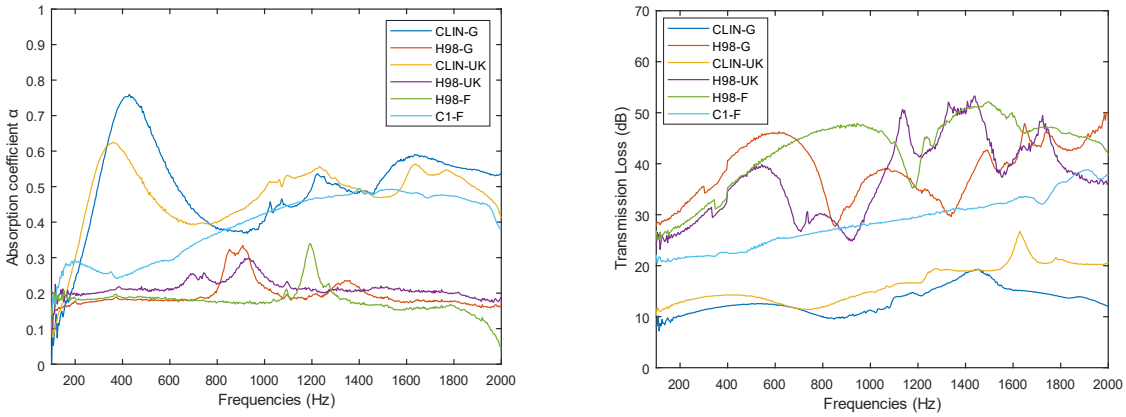

Fig. 4: Sound absorption coefficient (left) and Transmission Loss coefficient (right) of the composites CLIN-G, H98-G, CLIN-UK, H98-UK, H98-F and C1-F.

It can be observed from Fig. 2 that sunflower pith presents very good sound absorbing properties, especially around 950 Hz, where it reaches an absorption coefficient of 1. It can also be observed that hemp shiv is a sound absorbing material almost as good as pith. The pith sample S shows a secondary peak at 1200 Hz in absorption that also appears in transmission loss, which may be due to localized elastic effects. It is noted that sunflower pith shows a higher transmission loss than hemp shiv, which remains nevertheless limited. At low frequencies, TL tends to 0-2 dB and, in the frequency range between 400 and 2000 Hz, TL remains very stable around 6 dB for pith and 3 dB for hemp shiv, which is quite low for building materials. However, the tested thickness is 5 cm, which is well below common wall thicknesses (which oscillate between 20 and 30 cm). Whilst (Glé, 2013) found that, for a group of hemp shiv samples, the denser ones had higher absorption and transmission loss coefficients, the results obtained in this study do not answer to the same principle, probably because they are two aggregates of different nature.

Regarding the composites C2-H*, C2-S and C2-H+S in Fig. 3, the absorption of the composites containing hemp shiv (C2-H* and C2-H+S) maintains the absorption behavior of the hemp shiv alone, with the only difference that the main peak appears around 650 Hz instead of 1000 Hz. On the other hand, the pith composite (C2-S) presents a maximum absorption of 0.6 at about 550 Hz, which remains acceptable. This inversion of the performance between pith and pith composite was also observed for thermal conductivity in (Abbas et al., 2020). While the tendencies of the absorption coefficient of C2-H* and C2-H+S are globally very close, the latter presents a certain noise that can also be appreciated for C2-S. This formulation has the highest TL coefficient, which varies between 10 and 20 dB. The Transmission Loss coefficient is also very close for C2-H* and C2-H+S and lower than that of C2-S, oscillating between 5 and 12 dB, which is too low to ensure the acoustic insulation of a building (we aim at a loss coefficient higher than 20 dB).

C2-H* and C2-H+S show a behavior quite similar to that of CLIN-G composite, which shows the absorption peak at about 400 Hz, and the behavior of C2-S is close to that of CLIN-UK, which shows an absorption peak at about 350 Hz. C1-F does not present the main peak as the previous composites do but maintains an absorption coefficient very close to CLIN-G and CLIN-UK's between 800 and 2000 Hz. The rest of the composites in Fig. 4, which contain H98 binder, a very impervious material due to the presence of closed porosity, show a fairly poor absorption that forms a plateau at 0.2 and a very interesting TL coefficient despite the signal noise. It can be noted that, at low frequencies, the absorption of the materials always tends to 0.1-0.2. Therefore, it can be concluded that the binder plays a major role in the acoustic behavior whilst the impact of the aggregate is more limited.

3.2 Discussion

The same Kundt's tube test allows the determination of several geometrical parameters of the porous media following the aforementioned procedure. These parameters are the air resistivity σ, the interparticle porosity ϕ_{inter}, the tortuosity α_∞, the viscous characteristic length Λ and the thermal characteristic length Λ'.

These results have been compared to the mechanical and hygrothermal parameters found in (Abbas et al., 2020) for C2-H*, C2-S and C2-H+S and it has been noted that two composites – C2-H* and C2-H+S – present very similar geometrical parameters (see Tab. 3) and very similar hygrothermal properties, namely the thermal conductivity λ, the vapor resistance μ and the practical Moisture Buffering Value $MBV_{practical}$ (see Tab. 4). This finding could suggest that similar microstructures yield similar macroscopic hygrothermal behaviors, at least when a common binder is used.

Tab. 3: Summary of the results of the geometrical parameters

Formulation	σ [N.s/m^4]	α_∞ [-]	Λ (x10^{-5} m)	Λ'(x10^{-5} m)	ϕ_{total} [-]	ϕ_{inter} [-]	ϕ_{intra} [-]
C2-H*	11625	3.56	12	31	0.70	0.41	0.49
C2-H+S	14500	3.44	10	33	0.70	0.43	0.48

Tab. 4: Summary of the hygrothermal properties from (Abbas et al., 2020)

Formulation	λ [W/(m.K)]	μ [-]	$MBV_{practical}$ [g/(m²·%HR)]
C2-H*	0.15	3.9	1.63
C2-H+S	0.14	3.9	1.71

In the aim of establishing more explicit correlations between acoustic and hygrothermal parameters, a cross-referenced analysis has been conducted, whose results are presented in (Abbas et al., 2021). Two correlations were found: the first was a decreasing power-law between the thermal conductivity and the interparticle porosity and the second was an exponential law between the water vapor permeability and the air permeability. We now seek to compare the experimental relationship between λ and ϕ_{inter} to several conductivity models for porous media from literature.

If we consider the material as a two-component composite in which each component, the solid matrix and the air in our case, is homogeneous, the thermal conductivity of the composite or "effective thermal conductivity" λ_e is known to be limited by the series and the parallel models. The series model, represented by Eq. (14), would be the lower limit and it describes the heat conduction in the material in a hypothetical case in which both phases are completely separated by a plane that is perpendicular to the direction of the heat flux.

$$\lambda_e = \frac{1}{\frac{1-\phi}{\lambda_s}+\frac{\phi}{\lambda_a}} \tag{14}$$

Where ϕ is the volume fraction of the second phase (the porosity in our case) and λ_s and λ_a are respectively the thermal conductivity of the solid phase and of the air.

The parallel model, on the other hand, represents the upper limit and describes the heat conduction in the case in which both phases are completely separated by a plane that is parallel to the direction of the heat flux and they do not interact with each other:

$$\lambda_e = (1-\phi)\cdot\lambda_s + \phi\cdot\lambda_a \tag{15}$$

These two models represent a very simplistic composite and are not expected to be adapted to reality but to establish the lower and higher possible values of the thermal conductivity of a two-phase material.

If $\lambda_a \ll \lambda_s$, then the second term of Eq. (15) can be neglected, leading to Loeb's relation (Loeb, 1954):

$$\lambda_e = (1-\phi)\cdot\lambda_s \tag{16}$$

Maxwell-Eucken models (Eucken, 1932; Maxwell, 1954) are slightly more complex and represent a composite material with two phases. One phase is continuous and the other one is composed of spherical inclusions that are perfectly disperse, that is, they are never in contact with nearby inclusions. The first model, Eq. (17), describes the heat conduction in a composite in which the continuous phase has a more important thermal conductivity (the inclusions can be understood as bubbles and the continuous phase as a solid matrix), while the second model, Eq. (18), describes the conduction in the case of the continuous phase having a lower thermal conductivity than the inclusions. In our case, the inclusions would be particles and the continuous phase would be the air.

$$\lambda_e = \lambda_s \frac{2\lambda_s+\lambda_a-2(\lambda_s-\lambda_a)\phi}{2\lambda_s+\lambda_a+(\lambda_s-\lambda_a)\phi} \tag{17}$$

$$\lambda_e = \lambda_a \frac{2\lambda_a+\lambda_s-2(\lambda_a-\lambda_s)(1-\phi)}{2\lambda_a+\lambda_s+(\lambda_a-\lambda_s)(1-\phi)} \tag{18}$$

These two models, particularly the first one, seem more realistic, although the hypothesis of the inclusions being perfectly disperse is hardly applicable to the materials studied.

Another model (Machrafi & Lebon, 2015), derived from the percolation theory and therefore called "percolation model" proposes:

$$\lambda_e = \lambda_s\cdot(1-\phi)^3 \tag{19}$$

Lastly, the model called the Effective Medium Theory (EMT) (Kirkpatrick, 1973; Landauer, 1952) is used to predict the thermal conductivity of a material with two components randomly disposed in which none of them is imposed to be disperse or continuous. It is described by Eq. (20).

$$(1-\phi)\frac{\lambda_s-\lambda_e}{\lambda_s+2\lambda_e} + \phi\frac{\lambda_a-\lambda_e}{\lambda_a+2\lambda_e} = 0 \tag{20}$$

The adequacy of the different models has been assessed using the least square adjustment between the measured value of the thermal conductivity of the composites λ and the λ_e modelled for each material. For λ_a, we use the thermal conductivity of the air at 300 K, $\lambda_a = 0.0262$ W/(m.K). As for ϕ, it will represent the inter-particle porosity of the materials. Generally, models do not specify which type of porosity must be used and, since the correlation has been found between λ and ϕ_{inter}, it seems more logical to use the latter. As mentioned in (Abbas et al., 2021), a plausible explanation is that for the bio-based composites studied, which are known to have a double-scale porosity, only the bigger-scale pores have an influence on thermal properties. The only parameter

left, and consequently the parameter used for the adjustment, is the thermal conductivity of the solid phase λ_s. Since the goal is to apply a single relation for the group of materials, we accept the simplification that all the materials have the same λ_s. The results are shown in Fig. 5 and in Tab. 5.

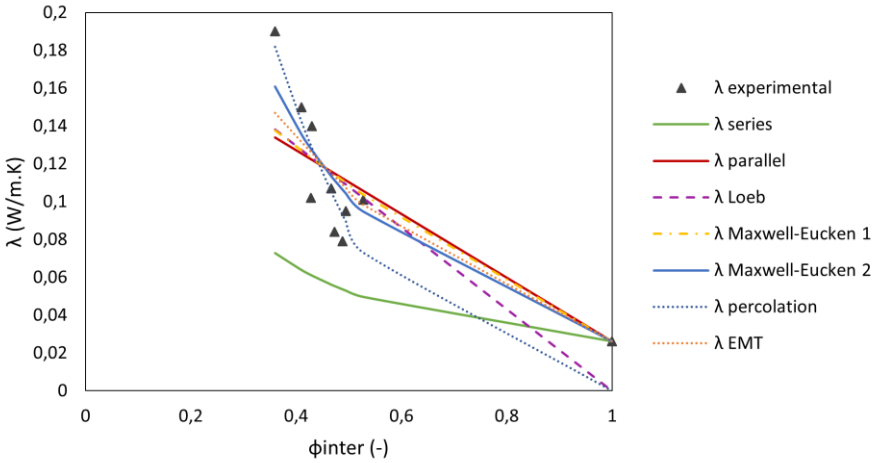

Fig. 5: Application of several models of the thermal conductivity of porous materials using the least square adjustment with λ_s as variable parameter

Tab. 5: Thermal conductivity of the solid phase and mean squared error (MSE) for each model

Model	λ_s [W/(m.K)]	MSE [-]
Series model	$1.879 \cdot 10^7$	0.00313
Parallel model	0.195	0.00058
Loeb's relation	0.216	0.00057
Maxwell-Eucken 1 model	0.227	0.00052
Maxwell-Eucken 2 model	5.906	0.00030
Percolation model	0.694	0.00025
Effective Medium Theory (EMT)	0.265	0.00042

From Fig. 5 it can be noted that Loeb's relation and the percolation model are not accurate for high porosity values. Tab. 5 reveals that the series model is not adapted to the experimental results and that the parallel model, the Maxwell-Eucken 1 model and the Effective Medium Theory yield λ_s values around 0,23 W/(m.K), which seem too low for a solid. Therefore, the only remaining model is Maxwell-Eucken 2, which adapts best to extreme porosity values, whose representation of the structure of the porous medium is the most realistic and which presents the second lowest mean squared error. Nevertheless, the lack of data for the thermal conductivity of the solid phase of bio-based composites prevents us from validating this model. Consequently, the most promising approximation to a model from literature remains Lichtenecker's formula, which was presented in (Abbas et al., 2021).

4 SUMMARY

This paper studies the acoustic behavior of sunflower pith and hemp shiv composites. It has been observed that both aggregates present a very good sound absorbing behavior, yet this trait is dampened in the presence of a binder. Furthermore, the binder is the main conditioning factor of both the absorption and the Transmission Loss coefficients. On the other hand, a possible relation between the geometrical parameters of the microstructure, which can be deduced from the acoustical measurements, and the macroscopic hygrothermal properties has arisen. For a common binder, composites with very similar microstructures seem to lead to very close values of thermal conductivity, vapor resistance and Moisture Buffering. Lastly, no thermal conductivity model among the ones studied is closer to the experimental correlation between the thermal conductivity and the interparticle porosity than Lichtenecker's formula, which was presented in (Abbas et al., 2021).

5 ACKNOWLEDGMENTS

This work has been supported by the French environmental and energy management agency (ADEME). The present work was performed within the framework of the LABEX CeLyA (ANR-10-LABX-0060) of Université de Lyon. The authors wish to thank Nadia Bekkouche and Tristan Cambonie for their technical support.

6 REFERENCES

Abbas, M. S., Gourdon, E., Glé, P., McGregor, F., Ferroukhi, M. Y., & Fabbri, A. (2021). Relationship between hygrothermal and acoustical behavior of hemp and sunflower composites. *Building and Environment*, *188*(October 2020). https://doi.org/10.1016/j.buildenv.2020.107462

Abbas, M. S., Mcgregor, F., Fabbri, A., & Ferroukhi, M. Y. (2020). The use of pith in the formulation of lightweight bio-based composites : impact on mechanical and hygrothermal properties. *Construction and Building Materials*, *259*. https://doi.org/10.1016/j.conbuildmat.2020.120573

Abbas, M. S., McGregor, F., Fabbri, A., & Ferroukhi, Y. (2019). Influence of origin and year of harvest on the performance of pith mortars. *3rd International Conference of Bio-Based Building Materials*, 42–48.

Ahmad, M. R., Chen, B., Haque, M. A., & Oderji, S. Y. (2020). Multiproperty characterization of cleaner and energy-efficient vegetal concrete based on one-part geopolymer binder. *Journal of Cleaner Production*, *253*. https://doi.org/10.1016/j.jclepro.2019.119916

Cambonie, T., & Gourdon, E. (2018). Innovative origami-based solutions for enhanced quarter-wavelength resonators. *Journal of Sound and Vibration*, *434*, 379–403. https://doi.org/10.1016/j.jsv.2018.07.029

Cérézo, V. (2005). *Propriétés mécaniques, thermiques et acoustiques d'un matériau à base de particules végétales : approche expérimentale et modélisation théorique*. http://theses.insa-lyon.fr/publication/2005isal0037/these.pdf

Chamoin, J. (2013). *Optimisation des propriétés (physiques, mécaniques et hydriques) de bétons de chanvre par la maîtrise de la formulation*. INSA de Rennes.

Champoux, Y., & Allard, J.-F. (1991). Dynamic tortuosity and bulk modulus in air-saturated porous media. *Journal of Applied Physics*, *70*, 1975–1979.

Cornaro, C., Zanella, V., Robazza, P., Belloni, E., & Buratti, C. (2020). An innovative straw bale wall package for sustainable buildings : experimental characterization , energy and environmental performance assessment. *Energy & Buildings*, *208*, 109636. https://doi.org/10.1016/j.enbuild.2019.109636

D'Alessandro, F., Bianchi, F., Baldinelli, G., Rotili, A., & Schiavoni, S. (2017). *Straw bale constructions : Laboratory , in fi eld and numerical assessment of energy and environmental performance*. *11*(April), 56–68. https://doi.org/10.1016/j.jobe.2017.03.012

Eucken, A. (1932). Die Wärmeleitfähigkeit Keramischer, Fester Stoffe – Ihre Berechnung aus der Wärmeleitfähigkeit der Bestandteile. *VDI Forschungsheft 353, Beilage Zu, Forschung Auf Dem Ggebiete Des Ingenieurwesens, Ausgabe B, Band 3*.

Glé, P. (2013). *Acoustique des Matériaux du Bâtiment à base de Fibres et Particules Végétales - Outils de Caractérisation, Modélisation et Optimisation* [ENTPE Lyon]. https://tel.archives-ouvertes.fr/tel-00923665

Gourdon, E., Chabriac, P.-A., Glé, P., Fabbri, A., & McGregor, F. (2015). Acoustical characterization and modelling of agricultural byproducts for building insulation. *First International Conference on Bio-Based Building Materials*, *33*(2), 449–453.

International Energy Agency, & UN Environment Programme. (2020). *2020 Global Status Report for Buildings and Construction*.

International Organization for Standardization. (2007). *ISO 8894-2:2007, Refractory materials - Determination of thermal conductivity - Part 2: Hot-wire method (parallel)*.

International Organization for Standardization. (2016). *NF EN ISO 12572:2016, Hygrothermal performance of building materials and products - Determination of water vapour transmission properties - Cup method*.

Iwase, T., Izumi, Y., & Kawabata, R. (1998). A new measuring method for sound propagation constant by using sound tube without any air spaces back of a test material. *Internoise 98*, 4.

Johnson, D. L., Koplik, J., & Dashen, R. (1987). Theory of dynamic permeability and tortuosity in fluid-saturated porous media. *Journal of Fluid Mechanics*, *176*, 379–402. https://doi.org/https://doi.org/10.1017/S0022112087000727

Kirkpatrick, S. (1973). Percolation and conduction. *Rev. Mod. Phys.*, *45*, 574–588.

Landauer, R. (1952). The electrical resistance of binary metallic mixtures. *J. Appl. Phys.*, *23*, 779–784.

Loeb, A. (1954). Thermal Conductivity : VIII , A Theory of Thermal Conductivity of Porous Materials. *Journal of the American Ceramic Society*, *37*(2), 96–99.

Lupíšek, A., Vaculíková, M., Mancík, S., Hodková, J., & Ržika, J. (2015). Design strategies for low embodied carbon and low embodied energy buildings: Principles and examples. *Energy Procedia*, *83*, 147–156. https://doi.org/10.1016/j.egypro.2015.12.205

Machrafi, H., & Lebon, G. (2015). Size and porosity effects on thermal conductivity of nanoporous material with an extension to nanoporous particles embedded in a host matrix. *Physics Letters, Section A: General, Atomic and Solid State Physics*, *379*(12–13), 968–973. https://doi.org/10.1016/j.physleta.2015.01.027

Maxwell, J. C. (1954). *A Treatise on Electricity and Magnetism* (third ed.). Dover Publications Inc.

McGregor, F., Heath, A., Fodde, E., & Shea, A. (2014). Conditions affecting the moisture buffering measurement performed on compressed earth blocks. *Building and Environment*, *75*, 11–18. https://doi.org/10.1016/j.buildenv.2014.01.009

Mnasri, F., Bahria, S., Slimani, M. E. A., Lahoucine, O., & El Ganaoui, M. (2020). Building incorporated bio-based materials: Experimental and numerical study. *Journal of Building Engineering*, *28*(October 2019). https://doi.org/10.1016/j.jobe.2019.101088

Olny, X., & Panneton, R. (2008). Acoustical determination of the parameters governing thermal dissipation in porous media. *The Journal of the Acoustical Society of America*, *123*(2), 814–824. https://doi.org/10.1121/1.2828066

Panneton, R., & Olny, X. (2006). Acoustical determination of the parameters governing viscous dissipation in porous media. *The Journal of the Acoustical Society of America*, *119*(4), 2027–2040. https://doi.org/10.1121/1.2169923

Rode, C., Peuhkuri, R. H., Mortensen, L. H., Hansen, K. K., Time, B., Gustavsen, A., Ojanen, T., Ahonen, J., Svennberg, K., & Arfvidsson, J. (2005). *Moisture Buffering of Building Materials*.

Utsuno, H., Tanaka, T., & Fujikawa, T. (1989). Transfer function method for measuring characteristic impedance and propagation constant of porous materials. *Journal of the Acoustical Society of America*, *86*(2), 637–643. https://doi.org/10.1121/1.398241

Zwikker, C., & Kosten, C. W. (1949). *Sound Absorbing Materials*. Elsevier Publishing Company.